Molecular Insights into the Electric Double-Layer Structure at a Polymer

Electrolyte-Electrode Interface

Aysha Siddika Asha^{1‡}, Justice Nkemakolam Iroegbu^{1‡}, Benjoe Rey B. Visayas², Maricris Mayes², Caiwei Shen^{1*}

¹Department of Mechanical Engineering, University of Massachusetts Dartmouth, Dartmouth,

MA, USA

²Department of Chemistry and Biochemistry, University of Massachusetts Dartmouth,

Dartmouth, MA, USA

[‡]These authors contributed equally

*Corresponding author:

Caiwei Shen

University of Massachusetts Dartmouth

285 Old Westport Road, Textile 211

North Dartmouth, MA 02747

Phone: +1-508-999-8449

Email: cshen2@umassd.edu

Abstract

Polymer electrolyte-based electric double-layer supercapacitors (EDLCs) have been increasingly studied for flexible, wearable, and multifunctional energy storage applications. Although the phenomenon that electrode materials present significantly lower EDL capacitances in polymer electrolytes than in liquid electrolytes has been widely observed, it has not been well studied and explained. Here we present the molecular dynamics simulation of a representative polymer electrolyte-based EDLC to reveal the atomic structure of such a polymer electrolyte-electrode interface for the first time. The polymer electrolyte composed of polyethylene oxide and lithium perchlorate is simulated between graphene electrodes and compared with an aqueous electrolytebased system with the same lithium salt. We find that the polymer-based system shows unique EDL structures in the inner and outer Helmholtz layers that are not seen in the aqueous one. Statistical analyses along with ab initio calculations show that the disparities mainly come from the different interaction strengths between ions, polymer or water molecules, and graphene electrodes. Despite these disparities, the intrinsic interfacial capacitances calculated from various simulated charge states of different EDLCs show very close values. Combined with experimental measurements, we conclude that the reduced capacitances with polymer electrolytes reported in the literature come from the poor interface between electrode and electrolyte, which can be significantly improved through proper thermal treatments.

Keywords: electric double-layer; supercapacitor; polymer electrolyte; electrolyte-electrode interface; molecular dynamics simulation

1. Introduction:

1

2

3

4

5

6

7

8

9

10

11

12

13

14

15

16

17

18

19

20

21

22

23

Electric double-layer capacitors (EDLCs) using polymer-based electrolytes have been attracting research interest in recent years for energy storage applications in flexible and wearable electronics¹⁻⁵, as well as multifunctional structural components⁶⁻⁸. This is because the energy storage mechanism of EDLC is much safer and more cyclically stable than that of current lithiumion batteries⁹⁻¹¹. Moreover, EDLCs can be constructed by using intrinsically strong electrode materials (such as graphene, carbon nanotube, and carbon fibers 12-17) and tough polymer electrolytes (such as polymer gel electrolytes and bi-continuous structural electrolytes ^{18–22}) to attain the required durability and mechanical properties for these new applications. While polymer electrolytes are critical for many EDLCs under development, studies have reported that electrode materials present significantly lower EDL capacitances in polymer electrolytes than those in liquid electrolytes. For example, activated carbon electrodes show specific capacitances of 70-120 F g⁻¹ in organic solution and ionic liquid electrolytes²³, while a similar electrode material only shows a specific capacitance of 4 F g⁻¹ with a polymer electrolyte²⁴. Carbon nanotube electrodes provide specific capacitances up to 37 F g⁻¹ with aqueous and ionic liquid electrolytes^{25,26}, but a similar electrode only shows 0.088 F g⁻¹ with a polymer electrolyte²⁷. A graphite electrode that is immersed in an aqueous electrolyte²⁸ was reported to have a capacitance of 7 mF cm⁻² measured at 0.1V s⁻¹, but a similar electrode shows a capacitance of only 2 mF cm⁻² measured at the same condition when a polymer-based electrolyte is used²⁹. As the EDL capacitance is determined by the interfacial area between electrolyte and electrode multiplies by the intrinsic capacitance per interfacial area^{9,30}, the reduced capacitance can be attributed to two issues at the polymer electrolyte-electrode interface: (1) The polymer electrolyte may not fully "wet" the electrode surface like the liquid electrolytes do, which will result in

reduced interfacial area³¹. (2) The EDL structure at the interface is different from that in a liquid electrolyte, which will result in lower intrinsic areal capacitance. The first issue can be mitigated by designing electrodes with more accessible surface areas and/or applying specific processes (such as thermal treatments) to improve the contact between polymer electrolyte and electrode material. The second issue, however, determines the maximum capacitance an electrode material can possibly achieve with polymer electrolytes. Although it is critical, the EDL structure and the intrinsic areal capacitance in polymer electrolyte-based systems have not been systematically studied before. Unlike polymer electrolytes, the EDL structure associated with liquid electrolytes has been theoretically modeled, computationally simulated, and experimentally measured in many previous studies. The general pictures of the EDL structure in the liquid have been depicted by various theoretical models from Helmholtz to Gouy-Chapman-Stern to account for the distributions of ions and solvent molecules^{9,32}. More recently, computational studies using molecular dynamics (MD) simulations³³ have revealed more details in EDL structure at the atomic level that match experimental observations. For example, experimental work using atomic force microscopy³⁴ and MD simulations^{35–40} show that the EDL is wider and more complex than predicted by theoretical models. MD simulations can also reveal the EDL structure based on the nature of the ions/solvent molecules⁴¹, the charging dynamics of the EDLC^{37,42–44}, and the influences of different factors on the intrinsic EDLC values^{45–48}. Therefore, MD simulation is a powerful tool to reveal the EDL structure at the polymer electrolyte-electrode interface. An understanding of such a structure at the atomic level can explain the performance disparities between liquid electrolytes and polymer electrolytes in EDLCs and help predict the maximum achievable specific capacitance of EDLCs using polymer electrolytes.

24

25

26

27

28

29

30

31

32

33

34

35

36

37

38

39

40

41

42

43

44

45

Here we present the MD simulation of a representative polymer electrolyte-based EDLC to reveal the EDL structure in polymer electrolytes for the first time. We simulate a polymer electrolyte composed of polyethylene oxide (PEO) and lithium perchlorate (LiClO₄) between two graphene sheets and compare it with an aqueous electrolyte-based system with the same lithium salt. We find that the polymer electrolyte-based EDLC also shows inner and outer Helmholtz layers but with unique structures. The unique EDL structures arise from different interaction strengths between ions, polymer molecules, and the graphene electrodes, as confirmed by ab initio calculations and analyses of atomic details, such as layer thicknesses and ion/atom concentrations. Though with different EDL structures, the calculated intrinsic interfacial capacitances of the polymer electrolyte-based system show very close values to that of the aqueous one. Combined with experimental measurements, we conclude that electrode materials with polymer electrolytes can achieve similar intrinsic interfacial capacitances to those with liquid electrolytes. The major reason that leads to reduced specific capacitances with polymer electrolytes reported in the literature is the decrease in interfacial area between the electrode and the electrolyte.

2. Model and Methodology:

2.1 Simulation details

2.1.1 Molecular Dynamics Simulations

Two representative systems were built to compare the differences between liquid electrolyte-based EDLCs and polymer electrolyte-based EDLCs. The control system was an aqueous electrolyte-based EDLC with 7200 water molecules, 128 Li⁺ ions, and 128 ClO₄⁻ ions forming the electrolyte between two pieces of single-layer graphene electrodes (Figure 1a). The other was a polymer electrolyte-based EDLC system consisting of the same species except that the water molecules were replaced with 22 chains of polyethylene oxide (PEO) molecules with 150 monomers per

chain (Figure 1b). The dimension of the electrode was 60.50 Å by 58.52 Å with 1400 carbon atoms in each graphene electrode. The distance between the electrodes was determined after equilibration run as detailed below.

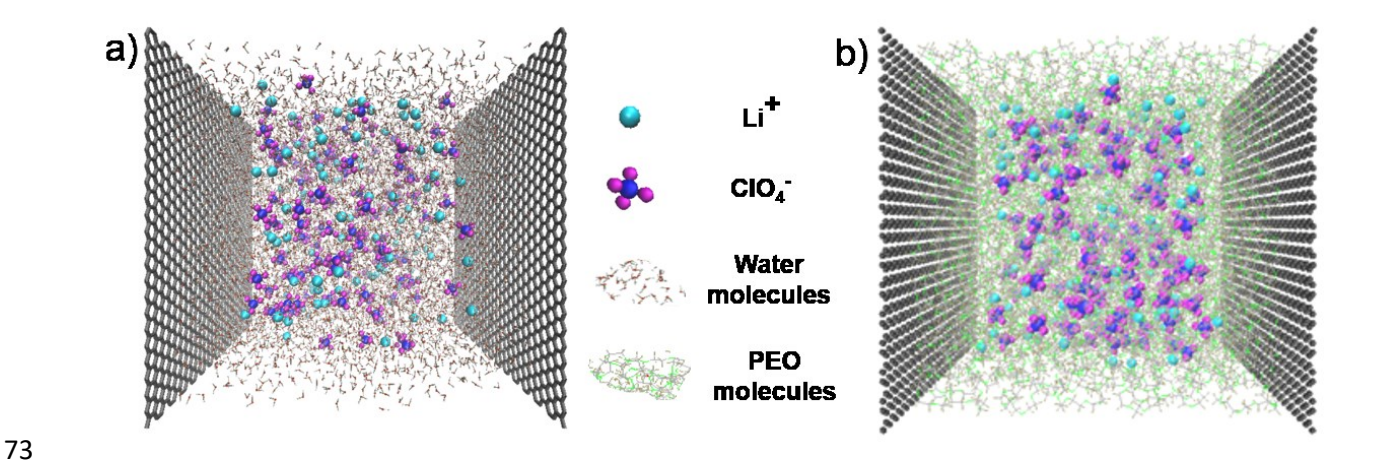


Figure 1. Snapshots of the simulation systems for (a) aqueous electrolyte-based EDLC and (b) polymer electrolyte-based EDLC.

The lithium perchlorate salt was modeled using the parameters based on Universal Force Field⁴⁹ parameters. The water model was the commonly used SPC/E. The SPC/E water parameters along with the graphene parameters were used as obtained from the Moltemplate website⁵⁰. All simulations were performed using the molecular-dynamics simulation code LAMMPS⁵¹ and CHARMM Generalized Force Field⁵² with the application of Lorentz-Berthelot mixing rules to determine cross-species interactions and a time step of 2 fs. The cut-offs for all non-bonded interactions and electrostatic interactions were 10 Å. The long-range electrostatic interaction was solved using the multilevel summation method⁵³. Both systems were minimized first by the steepest descent algorithm. Then the aqueous and polymer electrolyte systems were equilibrated for 1 ns and 2 ns respectively by NPT (constant number of particles, constant pressure, and constant temperature) simulation. The converged value of temperature and energy versus time graphs in

Supplementary Figure S1 proves the equilibrium conditions for the EDLCs. After that, NVT (constant number of particles, constant volume, and constant temperature) simulations were used for the production run. The positions of the carbon atoms relative to the plane of the electrode was kept constant by setting the force on each atom to zero throughout the NPT equilibration. The position of the electrode, however, was allowed to relax along the z-direction in order to equilibrate the density of the systems. The system, is periodic in all axes and in order to restrict interactions between the electrodes, a 30 Å vacuum was placed behind each electrode for a total of 60 Å separation between images. The equilibrated systems which resulted to a 65 Å distance between the two electrodes, were then simulated using the NVT ensemble for the production run. To determine the simulation temperature, we tested that the polymer electrolyte with 10 wt% LiClO₄ in PEO had a melting point of around 339 K (see the differential scanning calorimetry results in Supplementary Figure S2). We simulated both aqueous and polymer electrolytes at 350 K (referred to as the "aqueous system" and the "melted polymer system", respectively, in the following sections) to compare them in the liquid state, and then simulated the polymer electrolyte at 330 K (referred to as the "solid polymer system" in the following sections) to compare its behavior at a lower temperature. It should be noted that the simulation model only includes an amorphous phase that does not have a melting point. This "solid polymer system" only represents the amorphous part of the solid-state semi-crystalline electrolyte at 330 K. The polymer electrolyte was not simulated at a lower temperature such as room temperature because it took a much longer time to reach equilibrium. The aqueous system was simulated for 6 ns (3 million steps) and both polymer systems were simulated for 30 ns (15 million steps) to reach a stable ion distributions in the production run using the Nosé-Hoover thermostat. To simulate the EDL structure under various electric potentials, we used the constant charge method on the electrode as studies show a

87

88

89

90

91

92

93

94

95

96

97

98

99

100

101

102

103

104

105

106

107

108

negligible difference in EDL structure between the constant surface charge method and the constant electric potential method, especially at the low electric potential^{54,55}. Moreover, the constant potential method is more computationally expensive^{56,57}. We simulated all the above systems when ± 0 , ± 2.5 , ± 5.0 , ± 7.5 , and ± 10 electron charges per thousand carbon atoms (e/1000C) were applied on the graphene electrodes, respectively. We always applied negative charges on the left electrode (referred to as the negative electrode) and positive charges of the same amount on the right electrode (referred to as the positive electrode).

2.1.2 Ab initio calculations

To approximate the interaction energies of the systems under study, we selected regions from trajectory endpoints for both aqueous and polymer systems as representative structures of a subsystem containing an electrode, ion, and solvent molecules based on a 10 Å distance cutoff from the electrode. Structures were then fixed by capping free covalencies with hydrogen atoms. On these subsystems, we performed ab initio calculations using RHF/6-31G** and the converged wavefunctions were subjected to a Natural Energy Decomposition Analysis (NEDA)⁵⁸⁻⁶⁰ of the natural bonding orbitals (NBO) as implemented in GAMESS⁶¹ with the NBO6⁶² extension. The fragmentation was done in a manner where three fragments were assigned to groups 1. ion, 2. electrode, and 3. solvent (see Supplementary Figure S3).

2.2 Experimental details

In this section, experiments using both aqueous and polymer electrolytes were performed to validate some of the simulation results.

The aqueous electrolyte was prepared by mixing de-ionized water and lithium perchlorate (LiClO₄) salts obtained from Sigma-Aldrich. 1.068 g LiClO₄ was dissolved in 10 ml de-ionized water to make a 1 M LiClO₄ solution. As perfect single-layer graphene electrodes similar to the

ones used in the simulation systems were difficult to prepare and handle experimentally, we used chemically inert gold-coated electrodes instead. The electrodes were prepared by thermal evaporation of a 100 nm-thick layer of gold on polyimide films. The aqueous electrolyte-based EDLC was constructed by immersing two symmetric gold-coated electrodes into the aqueous electrolyte (see the illustration in Supplementary Figure S4a).

The PEO- LiClO₄ polymer electrolyte was prepared by the solution casting method. In a typical process, 0.3 g LiClO₄ and 3 g of polyethylene oxide (PEO) powder were dissolved in 30 ml acetonitrile in a glass tube. The solution was prepared under magnetic stirring for 24 hours. The solution was then cast in a Teflon dish and dried at 60 °C within a glove box for 24 hours to obtain a thin film of the PEO-LiClO₄ electrolyte. To construct the polymer electrolyte-based EDLC, a piece of the thin film electrolyte was cut and sandwiched between two gold-plated electrodes (see the illustration in Supplementary Figure S4b).

The capacitances of the EDLCs were measured by cyclic voltammetry (CV) tests between -0.1 to 0.1 V at a scan rate of 10 mV/s and then calculated using the following equation, where C is the capacitance per area, I is the current, t is the time, V is the voltage window, and A is the area of the electrode:

$$C = \frac{\int_0^V I dt}{VA}$$

The ionic conductivities of the electrolytes were measured by Electrochemical impedance spectroscopy (EIS) over a frequency range of 0.1 Hz to 1 MHz. Then the ionic conductivities (σ) were obtained using the following equation with the area of the electrode (A), impedance value (Z_{re}), and thickness of the electrolyte (t) taken into consideration:

 $\sigma = \frac{t}{Z_{re} * A}$

Both the CV and EIS tests were conducted using a Gamry Reference 600 potentiostat in the temperature range from 298 K to 345 K.

3. Results and Discussions:

3.1. The evolution of EDL structures with time

The theoretical models for EDL state that counter-ions tend to build up and form charged layers near the electrode-electrolyte interfaces. According to the models, the Li⁺ ions tend to move towards the negative electrode positioned at 0 Å, and the ClO₄⁻ ions tend to move towards the positive electrode positioned at 65 Å in our simulation systems. As all our simulations start with all ions randomly distributed in the electrolytes, the formation of EDL will take different amount of time depending on the applied charge on electrodes and the ionic conductivity of the electrolyte. Figures 2 and 3 compare the time evolution of counter-ion concentrations near negative and positive electrodes, respectively, in the first 6 ns for all three systems. Different colors in the figures indicate the concentrations of Li⁺ ions near the negative electrode (Figure 2) and ClO₄⁻ ions near the positive electrode (Figure 3).

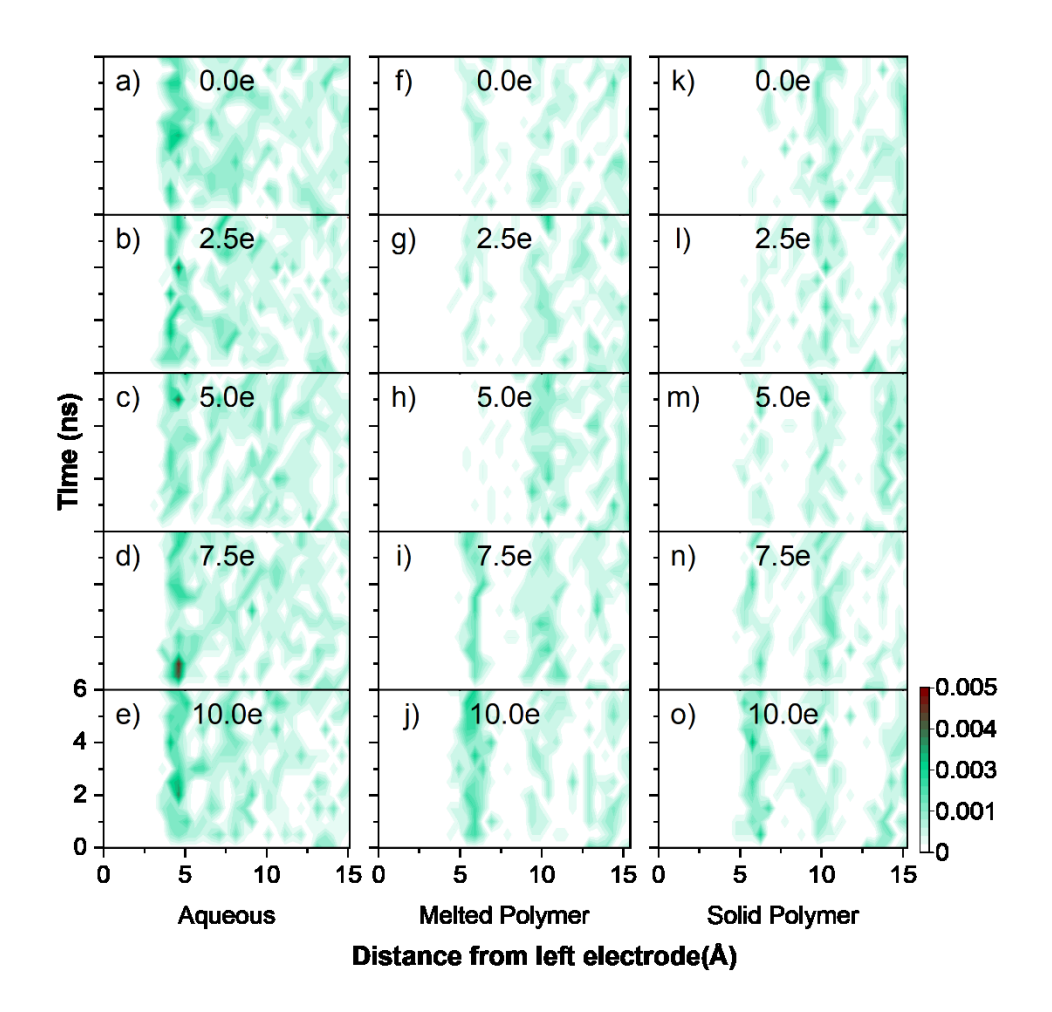


Figure 2: Heat maps showing the evolution of Li^+ concentration over 6 ns near the negative electrode under various charge conditions in three systems. Simulations are conducted with $\pm 0.0e$, $\pm 2.5e$, $\pm 5.0e$, $\pm 7.5e$, and ± 10.0 e/1000C on each electrode in (a-e) the aqueous system, (f-j) the melted polymer system, and (k-o) the solid polymer system. The colors indicate the concentration of Li^+ with the unit of ions per

 \mathring{A}^3 .

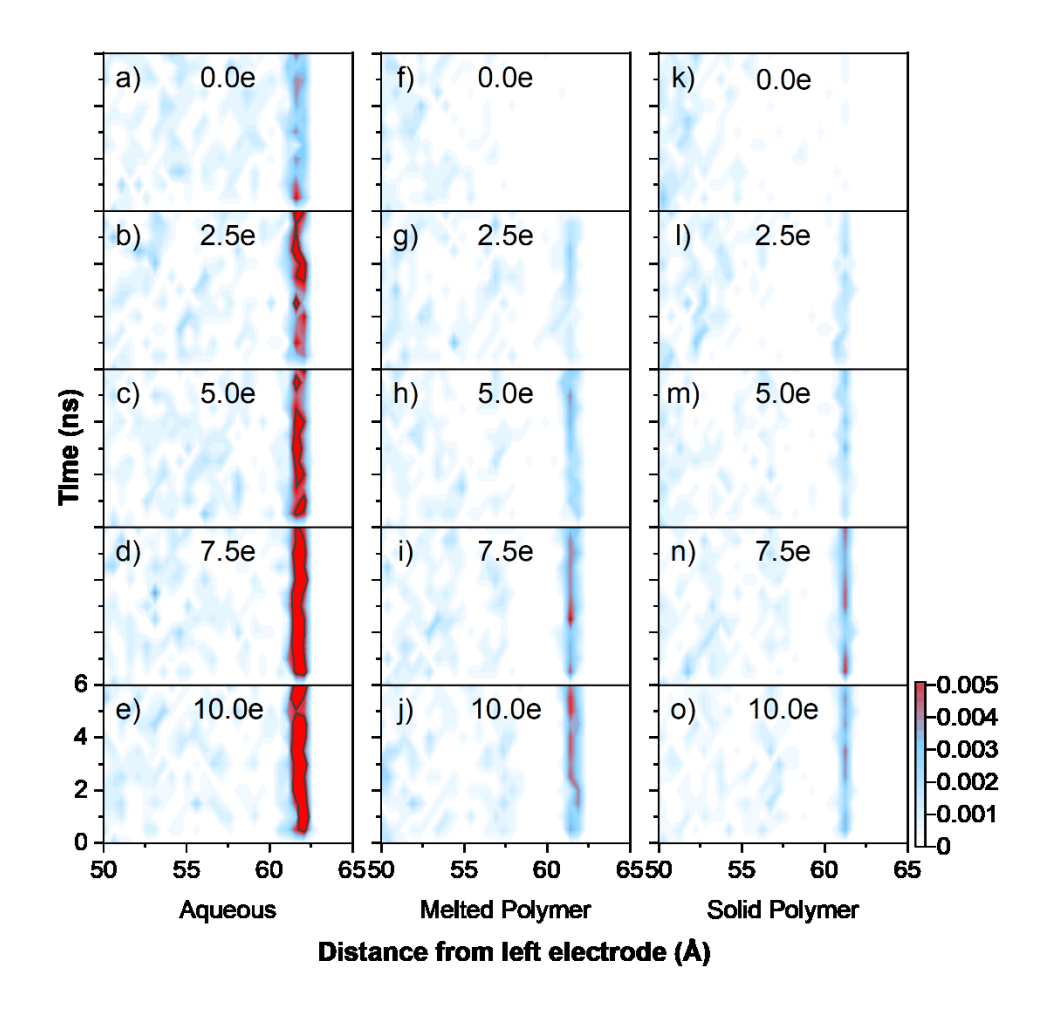


Figure 3: Heat maps showing the evolution of ClO_4^- concentration over 6 ns near the negative electrode under various charge conditions in three systems. Simulations are conducted with $\pm 0.0e$, $\pm 2.5e$, $\pm 5.0e$, $\pm 7.5e$, and ± 10.0 e/1000C on each electrode in (a-e) the aqueous system, (f-j) the melted polymer system, and (k-o) the solid polymer system. The colors indicate the concentration of ClO_4^- with the unit of ions P per \mathring{A}^3 .

In general, almost all sub-figures indicate the formation of ion layers near electrodes over time. Unlike theoretical models that only describe the EDL structure at equilibrium, the MD simulations show the dynamic movement of atoms at every time step, which leads to the fluctuation of ion concentrations in all figures. Despite some fluctuations, the peak concentration (highest number

density) of ions tends to reach the maximum value within 6 ns for the aqueous system while the accumulation of ions continues for both polymer systems, which justifies the different simulation times for different systems. The evolution of the peak concentration of ions with time at 10 e/1000C is also plotted in Supplementary Figure S5. The peak concentration of Li⁺ for the aqueous system fluctuates around a high value, while that for the polymer systems keeps increasing in the first 6 ns (Figure S5a). Similarly, the peak concentration of ClO₄- for the aqueous system starts to reach a stable value after about 4 ns, while that for the polymer system is still increasing (Figure S5b). The time evolutions of the total charge density for the aqueous and solid polymer systems are also compared in Figure S5 c and d, showing similar results. These observations qualitatively show that the aqueous electrolyte has a much higher ion conductivity than the polymer ones as it takes much less time for the EDL to establish in the aqueous system. The results also show that the formation processes of EDL structures in the two polymer systems are very similar, except that the solid polymer electrolyte has a lower ionic conductivity and its EDL formation is slightly slower than the melted one. Figure S5e shows that the total charge distribution of the solid polymer system has only very minor fluctuations from 25 to 30 ns, justifying that 30 ns of simulation is sufficient to reach equilibrium for such a system.

Other interesting phenomena can be observed in Figures 2 and 3. When no charge (0 e/1000C) is applied to the electrodes, the aqueous system still has significant ion layers formed, as seen in Figures 2a and 3a. For the uncharged aqueous system, the formation of ion layers near the electrodes is driven by ion- π interactions, i.e. the attractions between ions and the graphene electrodes^{63–65}. While the simulation is using a non-polarized force field, such interactions are the results of the interactions between static charges and Lennard Jones potentials. But for both polymer systems, the Li⁺ ions (Figures 2f and 2g) and ClO₄⁻ ions (Figures 3f and 3g) are distributed

185

186

187

188

189

190

191

192

193

194

195

196

197

198

199

200

201

202

203

204

205

206

much further away from the electrodes, and no clear high-concentration ClO_4^- layers are formed. This also means that there is a considerably thick layer of polymer molecules attached to the surface of the electrodes. The fact that the polymer layers block the access of ions to electrode surfaces over the whole time scale indicates that the attractions between polymer molecules and the π bonds in graphene electrodes⁶⁶ are stronger than the ion- π interactions⁶⁷.

When the amount of charge applied on electrodes increases, the Li⁺ distributions in the aqueous system show a similar pattern to the uncharged case (Figures 2a to 2e). The Li⁺ distributions in the polymer systems, however, start to show clear ion layers, especially at high charge conditions (Figures 2f to 2o). The differences between the aqueous system and the polymer systems in terms of Li⁺ distribution at increased charge conditions indicate that the negative charges on the electrodes attract Li⁺ and water molecules alike, but have a relatively weaker attraction to PEO molecules. On the other hand, the ClO₄⁻ distributions in all three systems show the same trend when the electrode charge increases (Figure 3). A single layer of ClO₄⁻ is formed near the positive electrode and it shows higher ion concentrations at higher charge levels. This indicates that the positive charges on the electrodes have a much stronger effect on ClO₄⁻ ions than on water and PEO molecules.

3.2. The equilibrium EDL structures

As mentioned in the previous section, the EDL structure is always dynamic in MD simulations, but it can be considered to be in equilibrium when the peak concentration of ions starts to fluctuate around a stable value. The average number densities of all species over a long-enough time range should represent the equilibrium EDL structures of the simulated systems. Here, we consider Li⁺ and ClO₄⁻ as the solute and water or polymer molecules as the solvent in the electrolyte systems.

We plot the average number densities of solute ions and solvent atoms from 4 to 6 ns for the aqueous system and from 25 to 30 ns for the polymer systems in Figures 4 and 5, based on the different amounts of time needed for those systems to reach equilibrium.

Similar to the observations in Section 3.1, Figure 4a shows high ion concentrations near both electrodes due to the ion- π interactions even when no charge (0 e/1000C) is applied to the electrodes. It is clear that the peak concentration of ClO₄ is higher than that of Li⁺, which agrees with the previous studies 64,65 that the anion- π interactions are stronger than the cation- π interactions. There are also considerable interactions between water molecules and graphene electrodes, which results in an inner Helmholtz layer (IHL) formed by solvent molecules on the electrode surface as seen in Figure 5a. Based on the position of the concentration peaks of solvent atoms, we can estimate that the IHL is located at about 3.6 Å from the electrodes in the aqueous system, which agrees with previous MD simulations^{68,69}. This IHL prevents the hydrated cations and anions from moving towards the charged graphene surface 70,71 and results in the first concentration peaks of ions, i.e. the outer Helmholtz layer (OHL), located behind this layer. Here, the OHL formed by Li⁺ is about 4.6 Å, and that formed by ClO₄⁻ is about 4.1 Å from the electrodes. The cation- π and anion- π interactions are diminished in the polymer systems as seen in Figures 4 f and k, in which the number densities of ClO₄ do not have clear peaks near both electrodes, and the peaks of Li⁺ are far away from the electrodes. The explanation that this is caused by a stronger polymer- π interaction can be confirmed by Figures 5 f and k, in which peaks of atoms in polymer molecules are seen near the electrodes. The polymer molecules are clearly polarized (i.e. with separation of positive and negative charges inside molecules) near the electrodes, as the hydrogen peaks which carry positive partial charges are closer (about 3.0 Å) to and the oxygen peaks which

230

231

232

233

234

235

236

237

238

239

240

241

242

243

244

245

246

247

248

249

250

carry negative partial charges are farther away (about 4.5 Å) from the electrodes. These polarized molecules form a thick IHL, making the closest OHL formed by Li⁺ about 6.0 Å from the electrodes.

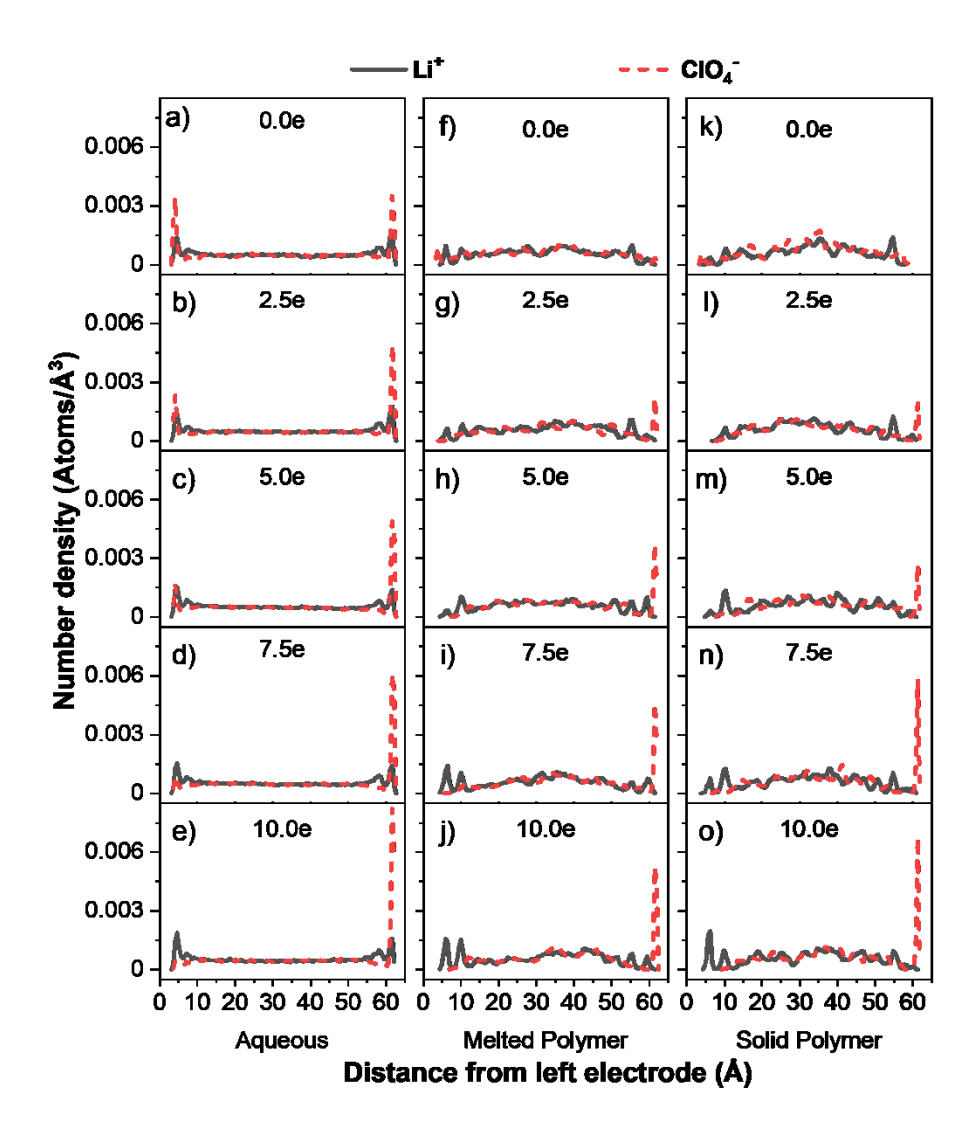


Figure 4: Equilibrium number density distributions of Li^+ and ClO_4^- ions under various charge conditions. Simulations are conducted with $\pm 0.0e$, $\pm 2.5e$, $\pm 5.0e$, $\pm 7.5e$, and ± 10.0 e/1000C on each electrode in (a-e) the aqueous system, (f-j) the melted polymer system, and (k-o) the solid polymer system.

When the applied charge on electrodes increases, all three systems show the same trend that the concentration of counter ions towards the respective electrode increases and that of co-ions decreases. In the aqueous system, the positions of OHLs formed by both ions (Figures 4 b to e) do not change much, and so do the positions of IHLs formed by water molecules (Figures 5 b to e). However, the change of charge has a significant effect on the peak concentrations of ClO₄ near electrodes. The anions are expelled from the negative electrode and attracted by the positive electrode. The peak concentrations of Li⁺, on the other hand, are also affected by the charge condition, but less significantly. The trends of how peak concentrations of ions change with the applied charge on electrodes are also compared in Supplementary Figure S6. Besides the first concentration peak of Li⁺, another smaller peak of the same ion can be seen under all charge conditions. This is caused by the over-screening effect, in which the charge of an ion layer exceeds the total charge on the electrode and subsequent layers of alternating charge (caused by both ions and polarized solvent molecules) form until the electrode charge is completely balanced³³. This "concentration oscillation" phenomenon is commonly reported in liquid electrolytes^{42,72–74}. The phenomenon is more obvious for Li⁺ than for ClO₄⁻, because Li⁺ ions are associated with more solvent molecules and tend to be over-screened by these polarized molecules. In comparison, the ClO₄ ions are less associated with solvent molecules. To evaluate the degree of association between Li⁺ ions and water molecules (represented by the oxygen atoms in water, denoted as O_w), we can consider the radial distribution function (RDF) of O_w around Li⁺ (denoted as RDF: Li⁺-O_w), which is computed as the average number density of O_w as a function of distance from Li⁺ ions in the aqueous system. Similarly, the RDF between ClO₄⁻ and O_w can be computed. The computed RDFs, as well as their integrations which represent the cumulative coordination

260

261

262

263

264

265

266

267

268

269

270

271

272

273

274

275

276

277

278

279

280

numbers of solvent molecules around ions, are plotted in Supplementary Figure S7. The high peak at 2.0 Å for RDF: Li⁺–O_w (Figure S7a) indicates a strong association between Li⁺ and O_w, while a relatively small peak for RDF: ClO₄⁻–O_w (Figure S7b) is seen at around 4.0 Å. The integrations of RDFs show that each Li⁺ is associated with approximately 4 O_w within a radius of 2.0 Å, while each ClO₄⁻ ion is associated with 3.7 O_w within 4.0 Å.

In the two polymer systems, the peak concentrations of ions behave in a similar way when the applied charge increases, as seen in Figures 4 g to j and l to o, as well as in Supplementary Figure S5. The differences between the melted and solid polymer systems are minor. However, the OHL structures formed by ions are distinct from those seen in the aqueous system.

For the OHLs formed by Li⁺ near the negative electrode, two concentration peaks positioned at about 6.0 Å and 10.0 Å in the melted polymer system, and 6.25 Å and 10.25 Å in the solid polymer system, respectively, can be seen. Different from the concentration oscillation of Li⁺ observed in the aqueous system, the second peak here is similar to or even higher than the first peak. An explanation is that Li⁺ ions are highly associated with the oxygen atoms in PEO molecules (denoted as O_p)^{67,75–77} as illustrated in Supplementary Figure S8. The charge provided by the first Li⁺ layer is over-screened by the polarized polymer shell and a significant second ion layer is needed to neutralize the excess charge caused by the over-screening effect. This is confirmed by the RDF of around Li⁺ (denoted as RDF: Li⁺– O_p) shown in Figure S7c, which has a high peak at 2.0 Å. The integrations of RDFs show that each Li⁺ is associated with approximately 5 O_p within 2.0 Å in the polymer systems, even more than the 4 O_w in the aqueous system.

For the OHLs formed by ClO₄⁻, the positions are at about 3.5 Å in the melted polymer system and 3.75 Å in the solid polymer system from the positive electrodes, respectively. Compared to 4.1 Å

in the aqueous system, ClO_4^- layers are getting closer to the positive electrodes in the polymer systems. Considering that the polymer molecules form the same thick IHLs under various charge conditions (Figures 5 g to j and 1 to o), the ClO_4^- ions actually form OHLs that are inside IHLs near the positive electrodes, which is an unseen phenomenon in other liquid electrolytes with small solvent molecules. The phenomenon is caused not only by the large size of polymer molecules but also by the weak association between ClO_4^- ions and PEO molecules. The RDF of ClO_4^- - O_p (Figure S7d) shows a small peak at around 4.0 Å, and its integration indicates that each ClO_4^- ion is associated with only 0.8 O_p in the polymer systems at a distance of 4.0 Å.

In addition to IHL and OHL, the diffuse layer in which the concentration of solvent atoms fluctuates before reaching a stable value (Figure 5) ends at about 9 Å away from the electrodes in

the aqueous system, consistent with previous simulation and experimental studies^{78–83}. In the two

polymer systems, the diffuse layers end at over 15 Å away from electrodes, indicating much thicker

overall EDL structures.

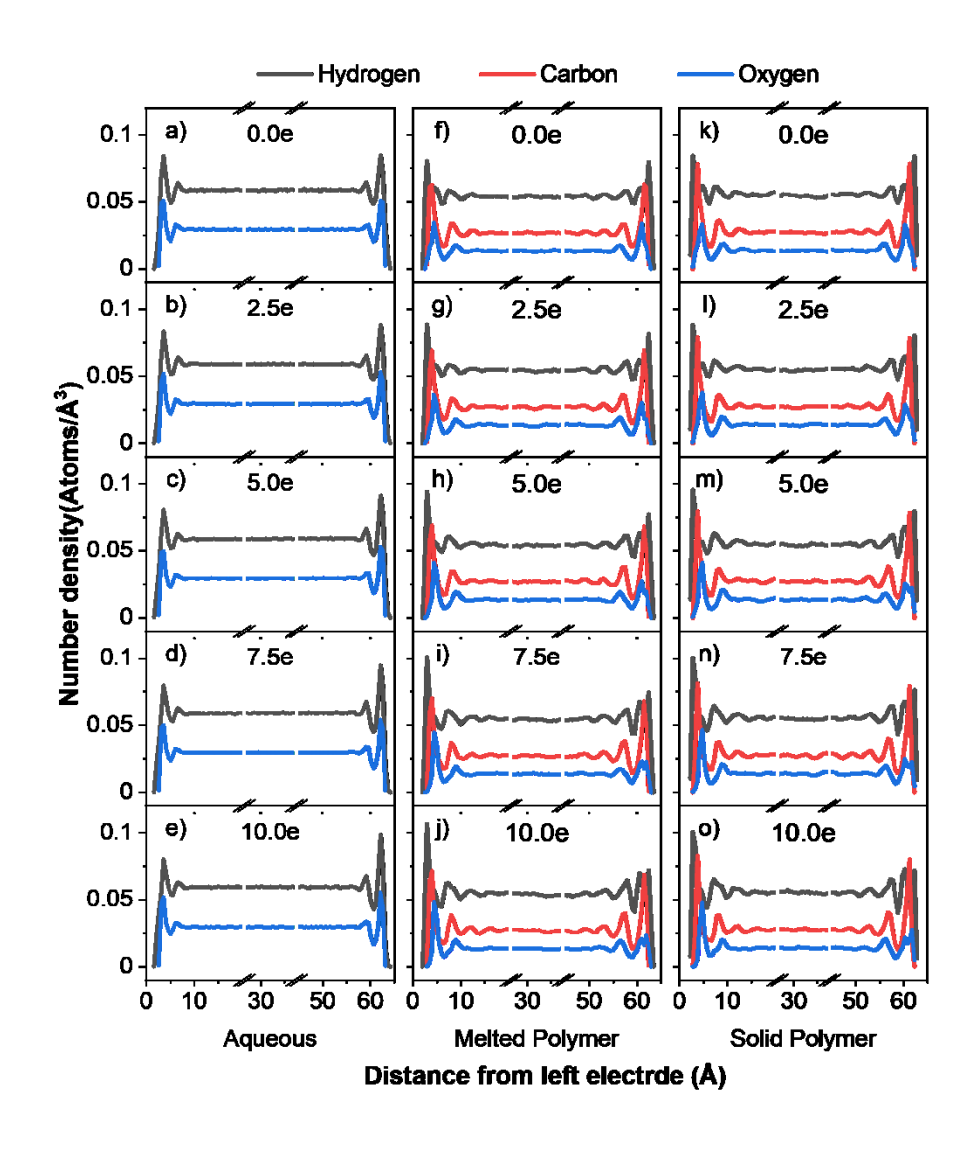


Figure 5. Equilibrium number density distributions of solvent atoms under various charge conditions. Simulations are conducted with $\pm 0.0e$, $\pm 2.5e$, $\pm 5.0e$, $\pm 7.5e$, and ± 10.0 e/1000C on each electrode in (a-e) the aqueous system, (f-j) the melted polymer system, and (k-o) the solid polymer system.

Ab initio calculations using NEDA were conducted to gain a better understanding of the equilibrium EDL structure. The energy decomposition values from NEDA have been shown in Supplementary Table S1 and plotted in Supplementary Figure S9. The total energies of Li⁺_(aq) and

CIO₄⁻ (aq) sub-systems from the aqueous system are -133.53 kcal/mol and -30.99 kcal/mol respectively while the total energies of Li⁺ (PEO) and ClO₄⁻ (PEO) sub-systems from the polymer system are -156.09 kcal/mol and -3.77 kcal/mol respectively (Supplementary Table S1). From these total energy values, the use of PEO increases the interaction energies of the Li⁺ ion while decreasing the interaction energies of the ClO₄⁻ ion. Moreover, these differences in interaction energies of Li⁺ and ClO₄⁻ justify their layer formations in the two different systems. Since ClO₄⁻ does not interact as much as Li⁺ with the solvent and electrode in both aqueous and polymer systems, its layer formation is more a result of its attraction towards the positive electrode. This explains the higher number density and higher concentration of ClO₄⁻ ions near the positive electrode in both systems. On contrary, Li⁺ interacts more with solvent molecules. It has a larger solvation shell in the aqueous system and is in a chelated state in the polymer system which can hinder its attraction with the negative electrode. The highest total energy of Li⁺ (PEO) in the polymer system and the structure of PEO molecules can also rationalize the double peaks observed as the regions near the electrode with the maximum number of Li⁺-O_(PEO) "chelation" regions.

To summarize the above discussions and analyses, we create the illustration in Figure 6 to show the unique features of the equilibrium EDL structure of the polymer system. First, the structure has thick IHLs formed by polarized PEO molecules with hydrogen atoms attached to the electrodes, carbon atoms, and then oxygen atoms forming two layers after that. Second, on the negative electrode side, two significant OHLs formed by Li⁺ ions are next to the IHL. Unlike the EDL structures in liquid electrolytes where the ion concentrations decrease with the distance from electrodes, this structure can have more ions in the second OHL. Third, on the positive electrode side, the OHL formed by CLO₄⁻ ions is located inside the IHL, while the OHLs are always outside the IHLs in liquid electrolytes.

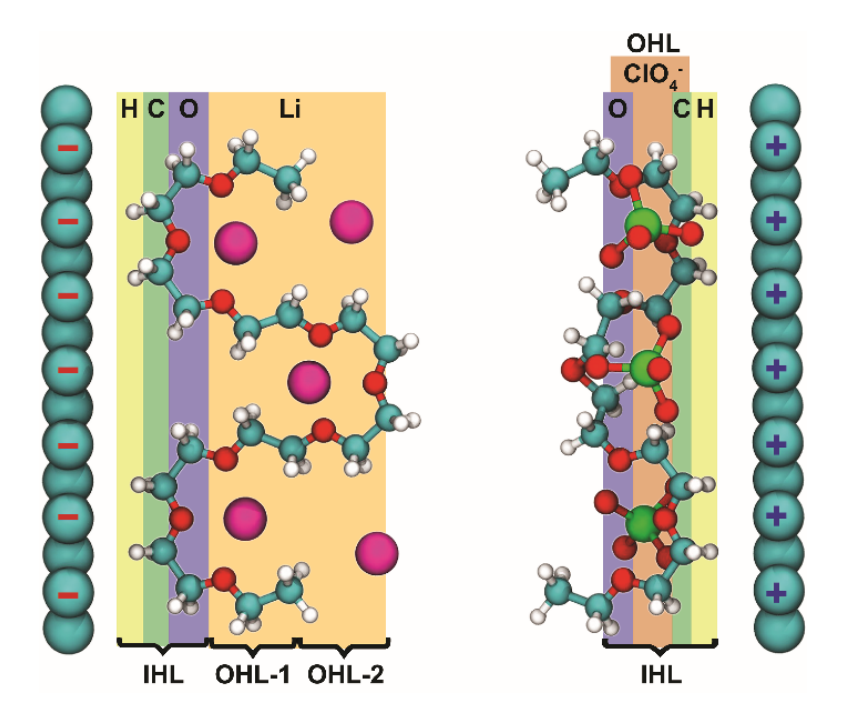


Figure 6. Illustration of the equilibrium EDL structure of the polymer electrolyte-based EDLC showing 351 the distinct features that are different from liquid electrolyte-based ones.

353

354

355

356

357

359

360

361

352

350

3.3. Interfacial capacitance and experimental verification

With the results from the simulated equilibrium EDL structures, we can find out the equilibrium EDL capacitance of the two-electrode system (C) under each charge condition according to the equation below:

$$C = \frac{\Delta Q}{\Delta V}$$

where ΔQ is the amount of charge applied on each electrode and ΔV is the voltage or potential difference between positive and negative electrodes. To find out the potential difference, we used the total charge density distribution between two electrodes and solved the one-dimensional Poisson's equation. The total charge density includes the charges from ions and polarized solvent molecules.

Supplementary Figure S10 compares the charge density distributions of the three systems when simulated with 0 e/1000C, ±2.5 e/1000C, ±5.0 e/1000C, ±7.5 e/1000C and ±10 e/1000C applied on electrodes. The plots also include the charge contributions from solvent atoms and ions, respectively. For all three systems with no charge applied, the charge distributions are symmetric as expected in such symmetric systems. The oscillation features are caused by the over-screening effect described in the previous section. Here, we can see that the oscillation of total charges is caused by both ionic charges and polarized solvent molecules, which agrees with previous studies⁸⁴. In the aqueous system Supplementary Figure S10a, the net charges from solvent (water) molecules contribute significantly to the total charge, whereas in both polymer systems Supplementary Figure S10f and S10k, the contribution from polarized polymer molecules is even more dominating. When the three systems are charged we can see that the solvent molecules become more polarized near the negative electrode and less so near the positive electrode. The charge contribution from ions, on the other hand, is more significant near the positive electrode, thanks to the ClO₄⁻ distribution as discussed in the previous section. The major difference between the aqueous system and the polymer systems is that the charge layers are much thicker in the polymer systems, which agrees with the EDL thickness analyzed in the previous section.

380

362

363

364

365

366

367

368

369

370

371

372

373

374

375

376

377

378

379

381

382

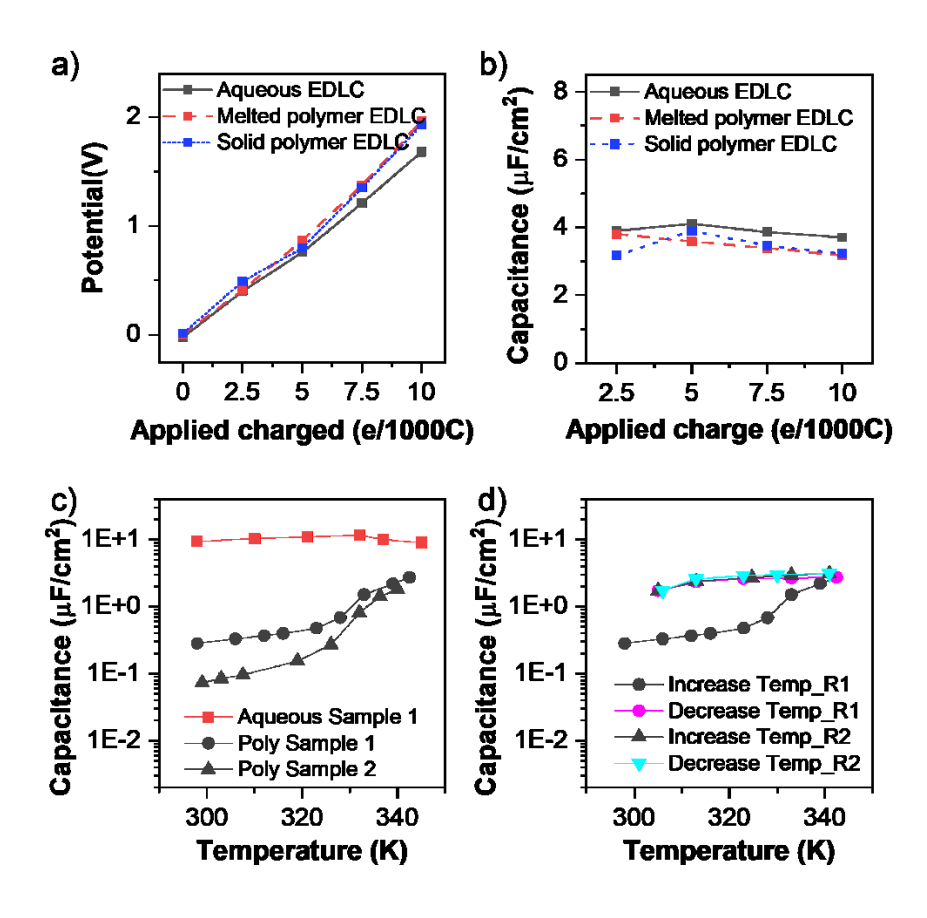


Figure 7. (a) The potential difference between positive and negative electrodes as a function of applied charge on electrodes for all three simulated systems. (b) The capacitance as a function of applied charge on electrodes for all three simulated systems. Experimentally measured capacitances of the gold electrodes: (c) with the aqueous electrolyte and two polymer electrolyte samples at different temperatures, and (d) with the same polymer electrolyte sample during two heating-cooling cycles.

Increase/decrease Temp_R1/2 indicates the 1st/2nd round of the heating/cooling cycle of the test. The capacitances are plotted in log scale.

Figure 7a and 7b summarizes the potential differences and the capacitances as functions of applied charge for all systems (see the potential distributions calculated from the charge density distributions under various charge conditions in Supplementary Figure S11). The potential differences increase almost linearly with the applied charge for all the systems (Figure 7a). The

values are very close for the two polymer systems, which is the result of similar equilibrium EDL structures. The potential differences in the aqueous system are relatively smaller under every charge condition. As a result, the capacitance of the aqueous system is slightly higher than those of the polymer systems (Figure 7b). Specifically, the capacitance of the aqueous system ranges from 3.7 to 4.1 µF cm⁻², with an average value of 3.9 µF cm⁻². The capacitance of the melted polymer system ranges from 3.2 to 3.8 µF cm⁻², with an average value of 3.5 µF cm⁻², and that of the solid polymer system ranges from 3.2 to 3.9 µF cm⁻², with an average value of 3.4 µF cm⁻². The small deviations in the order of 0.1 µF cm⁻² can simply come from the dynamic behavior of EDL structure as discussed in Section 3.1, which can be mitigated by simulating the systems for a longer time and taking the average values (e.g. total charge density) over a longer time range. But the surprising result here is that the electrodes contacting with a polymer electrolyte, whether in a melted liquid state or a solid state, show capacitances that are similar to the same electrodes contacting with an aqueous electrolyte. This seems to be contradictory to conventional experimental results where we see aqueous EDLCs showing capacitances of orders of magnitude higher than those of the polymer electrolyte-based EDLCs, as discussed in the introduction section. Possible explanations include that the simulation systems only consider the perfectly flat electrodes in perfect contact with a purely amorphous polymer electrolyte and that the simulations are conducted at higher temperatures compared with previous experimental work. To understand the differences between simulations and experiments, we conducted experiments using inert and flat gold electrodes contacting with both aqueous electrolyte and polymer electrolyte. Figure 7c and 7d summarizes the experimental results of capacitance measurements. For the gold-

plated electrodes tested in the aqueous electrolyte (1 M LiClO₄) under temperatures between 298

K and 350 K, the capacitance does not change much with temperature and shows values between

396

397

398

399

400

401

402

403

404

405

406

407

408

409

410

411

412

413

414

415

416

417

9.1 and 11.7 µF cm⁻² (Figure 7c). Polymer electrolyte (PEO + 10 wt% LiClO₄) samples sandwiched between gold-plated electrodes are also tested within the same temperature range. The results of the two representative samples are plotted in the same figure. We find that every polymer electrolyte sample shows a different capacitance, which varies between the orders of 0.01 and 0.1 μF cm⁻² when initially tested at around 298 K (room temperature). However, the measured capacitance increases significantly when we increase the temperature, and all the samples achieve similar capacitances around 3 µF cm⁻² near the melting point of 339 K. Moreover, when we cool down the melted sample, the capacitance remains in the order of 1 µF cm⁻² and will not change much when we re-heat it and re-cool it (Figure 7d). This phenomenon can be explained by the illustration in Supplementary Figure S12. Every polymer electrolyte sample has a relatively poor and uncertain contact with the electrode in the micro/nanoscale at the initial solid state. Upon heating up to the melting point, the polymer electrolyte deforms or melts to fully cover the electrode surface and form a much better interface. Such interface is preserved during cooling and re-heating processes. The results indicate that inconsistent and extremely low EDL capacitances measured with polymer electrolytes are most likely due to the poor contact between the electrode and electrolyte on the micro/nanoscale. Moreover, the polymer electrolyte-electrode interface can be significantly improved and stabilized by heating and cycling the system between room temperature and the melting point of the electrolyte. Although the capacitance of the polymer electrolyte sample reaches a stable value of about 3 µF cm⁻² near the melting point, it is still a few times lower than that of the aqueous sample which has a capacitance of over 9 µF cm⁻² at the same temperature, unlike the prediction by the MD simulation that the polymer electrolyte-based EDLC shows very close capacitance values to the

aqueous electrolyte-based EDLC. This can be explained by the orders of magnitude difference in

419

420

421

422

423

424

425

426

427

428

429

430

431

432

433

434

435

436

437

438

439

440

the ionic conductivities of the two systems. The macroscopic experiments are more affected by the impedance of the EDLC device, which is inversely proportional to the ionic conductivity of the electrolyte. A lower capacitance will be measured when the ionic conductivity is too low, even if the ideal interfacial capacitance is similar. The ionic conductivities of the aqueous electrolyte and the polymer electrolyte are also estimated by MD simulations and characterized experimentally, as detailed in the following section.

3.4 Ionic conductivity and experimental verification

Figure 8 compares the ionic conductivities of the aqueous electrolyte and the polymer electrolyte obtained from both MD simulations and experiments. To compute ionic conductivity in MD simulation, mean square displacements (MSD) of ions have first been calculated from the first 5 ns production run. The cation and anion diffusion coefficients were then calculated from the slope of the time dependence of MSD using the following equation.

454
$$D = \lim_{t \to \infty} \frac{1}{6t} < |R_i(t) - R_i(0)|^2 >$$

In the above formulas, D is the diffusion coefficient, t is the time, $R_i(t)$ is the position of the ith ion at time t, and the brackets <> denote the ensemble average.

The diffusion coefficients are then used to determine ionic conductivities via the Nernst-Einstein Equation below:

459
$$\sigma^{NE} = \frac{e^2}{K_b T} (\rho_- q_-^2 D_- + \rho_+ q_+^2 D_+)$$

Here, e^2 represents the square of elementary charge, K_b represents Boltzmann's constant, T represents simulation temperature, ρ_+ and ρ_- represent the bulk density of cations and anions respectively, q_+^2 and q_-^2 represent cation and anion charge respectively. To obtain the ionic

conductivities at various temperatures, we re-simulated both aqueous and polymer systems from 298 K to 345 K.

For the aqueous electrolyte, both simulations and experiments show ionic conductivities of about 60 mS cm⁻¹ near 300 K and over 100 mS cm⁻¹ near 350 K. The agreement between experimental and simulation results validates the simulation parameters used for the aqueous system. For the polymer electrolyte, however, there are significant discrepancies between simulation and experimental results at low temperatures. The experimental ionic conductivities (~10⁻³ mS cm⁻¹) are more than one order of magnitude lower than the simulation ones (~10⁻¹ mS cm⁻¹) at low temperatures, but the experimental values increase sharply with the temperature and get close to the simulation values at high temperatures. A major reason for the steep increase of ionic conductivity is caused by the phase transition of the crystalline part of the polymer electrolyte⁸⁵. The X-ray diffraction characterization of our polymer electrolyte at various temperatures shows that the sample is semi-crystalline below 330 K and becomes completely amorphous or melted above 340 K (see Supplementary Figure S13). The simulation system, however, does not include any crystalline feature of the polymer, which is partially due to the small simulation box that is only about 6 nm in all dimensions. Nevertheless, both simulated and experimental ionic conductivities of polymer electrolytes are over two orders of magnitude lower than that of aqueous electrolytes, which can result in low measured capacitances in polymer electrolyte-based samples.

463

464

465

466

467

468

469

470

471

472

473

474

475

476

477

478

479

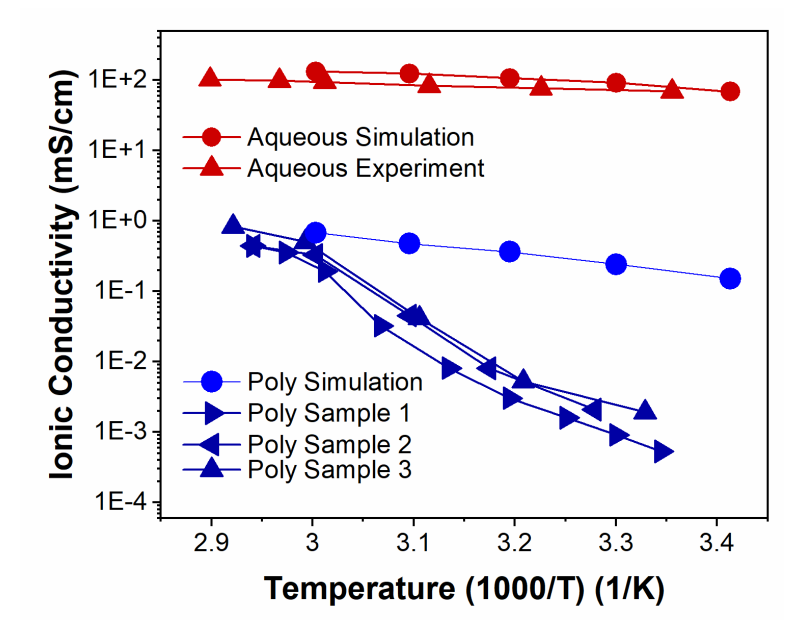


Figure 8. Comparison of the ionic conductivities of the aqueous electrolyte and the polymer electrolyte at different temperatures obtained from MD simulations and experiments.

4. Conclusions

In conclusion, the electric double-layer (EDL) structure at the polymer electrolyte-electrode interface is revealed through molecular dynamic simulations for the first time. The PEO-LiClO₄ electrolyte is simulated between two graphene electrodes at 350 K and 330 K, respectively, to reflect the different behavior of such electrolytes in a melted state and a solid state. The results are compared with an aqueous electrolyte-based system with the same lithium salt. The time evolutions of ion concentrations show that the polymer systems take longer time than the aqueous system to establish stable EDL structures due to the ionic conductivity discrepancy. After the EDL structures reach equilibrium, the polymer systems show thick inner Helmholtz layers formed by polarized PEO molecules, and outer Helmholtz layers formed by ions. The different layer thicknesses and ion/atom concentrations in the polymer and the aqueous systems are caused by the

different interaction strengths between ions, solvent (polymer or water) molecules, and graphene electrodes, as well as the distinct molecule sizes of PEO and water. Besides, there are two significant OHLs formed by Li⁺ near the negative electrode, and an OHL formed by CLO₄⁻ ions that is overlapping with the IHL near the positive electrode of the polymer system. Surprisingly, the intrinsic interfacial capacitances of the polymer systems are very close to the values of the aqueous system under the ideal simulation condition. Experimental measurements show that, although the capacitances measured with polymer electrolytes have low values at room temperature, much better capacitances approaching that measured with the aqueous electrolyte can be achieved when the polymer electrolytes are melted. The improved polymer electrolyte-electrode interfaces can be preserved during heating and cooling cycles. These results prove that EDLCs using polymer electrolytes can potentially achieve capacitances that are comparable to those using liquid electrolytes. Finally, the simulated ionic conductivities of both aqueous and polymer electrolytes are compared with experimental results, which validate the simulation parameters.

Conflicts of interest

There are no conflicts of interest to declare.

Acknowledgments

This research work is supported by UMass Dartmouth's Marine and Undersea Technology (MUST) Research Program funded by the Office of Naval Research (ONR) under grant number N00014-20-1-2170, and also supported by National Science Foundation grant 2217172. This research used the computing resources of the University of Massachusetts Green High-Performance Computing Cluster.

519

References

- 520 1. Jost, K., Dion, G. & Gogotsi, Y. Textile energy storage in perspective. J. Mater. Chem. A 2, 10776
- 521 (2014).
- 522 2. Huang, Q., Wang, D. & Zheng, Z. Textile-Based Electrochemical Energy Storage Devices.
- 523 Advanced Energy Materials vol. 6 1–28 (2016).
- 524 3. Zhai, S. et al. Textile energy storage: Structural design concepts, material selection and future
- 525 perspectives. *Energy Storage Mater.* **3**, 123–139 (2016).
- Liu, W., Song, M.-S., Kong, B. & Cui, Y. Flexible and Stretchable Energy Storage: Recent
- Advances and Future Perspectives. *Adv. Mater.* **29**, 1603436 (2017).
- 528 5. Muralee Gopi, C. V. V., Vinodh, R., Sambasivam, S., Obaidat, I. M. & Kim, H. J. Recent progress
- of advanced energy storage materials for flexible and wearable supercapacitor: From design and
- development to applications. *J. Energy Storage* **27**, 101035 (2020).
- 531 6. Xu, Y., Lu, W., Xu, G. & Chou, T.-W. Structural supercapacitor composites: A review. *Compos*.
- 532 Sci. Technol. 204, 108636 (2021).
- 533 7. Zhou, H. et al. Structural composite energy storage devices a review. Mater. Today Energy 24,
- 534 100924 (2022).
- 535 8. Chan, K. Y. et al. A critical review on multifunctional composites as structural capacitors for
- energy storage. *Compos. Struct.* **188**, 126–142 (2018).
- 537 9. Conway, B. E. Electrochemical supercapacitors: scientific fundamentals and technological
- 538 applications. (Springer Science & Business Media, 2013).
- 539 10. Miller, J. R. & Simon, P. MATERIALS SCIENCE: Electrochemical Capacitors for Energy

- Management. *Science* (80-.). **321**, 651–652 (2008).
- 541 11. Simon, P., Gogotsi, Y. & Dunn, B. Where do batteries end and supercapacitors begin? *Science* vol.
- 542 343 (2014).
- 543 12. Peng, X., Peng, L., Wu, C. & Xie, Y. Two dimensional nanomaterials for flexible supercapacitors.
- 544 Chem. Soc. Rev. 43, 3303 (2014).
- 545 13. Ke, Q. & Wang, J. Graphene-based materials for supercapacitor electrodes A review. *J. Mater.*
- **2**, 37–54 (2016).
- 547 14. Yang, Z. et al. Carbon nanotube- and graphene-based nanomaterials and applications in high-
- 548 voltage supercapacitor: A review. *Carbon N. Y.* **141**, 467–480 (2019).
- 549 15. Xie, S., Liu, S., Cheng, P. F. & Lu, X. Recent Advances toward Achieving High-Performance
- 550 Carbon-Fiber Materials for Supercapacitors. *ChemElectroChem* **5**, 571–582 (2018).
- 551 16. Cai, X., Zhang, C., Zhang, S., Fang, Y. & Zou, D. Application of carbon fibers to flexible,
- miniaturized wire/fiber-shaped energy conversion and storage devices. J. Mater. Chem. A 5, 2444—
- 553 2459 (2017).
- 554 17. Shen, C. et al. Wearable woven supercapacitor fabrics with high energy density and load-bearing
- 555 capability. Sci. Rep. 7, 14324 (2017).
- 556 18. Alipoori, S., Mazinani, S., Aboutalebi, S. H. & Sharif, F. Review of PVA-based gel polymer
- electrolytes in flexible solid-state supercapacitors: Opportunities and challenges. J. Energy
- 558 Storage **27**, 101072 (2020).
- 559 19. Wang, C. & Wallace, G. G. Flexible Electrodes and Electrolytes for Energy Storage.
- 560 *Electrochimica Acta* vol. 175 87–95 (2015).
- 561 20. Yu, Y. et al. Co-continuous structural electrolytes based on ionic liquid, epoxy resin and

- organoclay: Effects of organoclay content. *Mater. Des.* **104**, 126–133 (2016).
- 563 21. Tu, V. *et al.* Performance of bicontinuous structural electrolytes. *Multifunct. Mater.* **3**, 025001 (2020).
- Joyal, N., Chang, Y. C., Shonar, M., Chalivendra, V. & Shen, C. Solid polymer electrolytes with hydrates for structural supercapacitors. *J. Energy Storage* **51**, 104459 (2022).
- 567 23. Wei, L., Sevilla, M., Fuertes, A. B., Mokaya, R. & Yushin, G. Polypyrrole-Derived Activated
- Carbons for High-Performance Electrical Double-Layer Capacitors with Ionic Liquid Electrolyte.
- 569 Adv. Funct. Mater. 22, 827–834 (2012).
- 570 24. Hashmi, S. A. & and W. S. Schlindwein, R. J. Latham, R. G. L. Studies on all solid state electric
- double layer capacitors using proton and lithium ion conducting polymer electrolytes. *J. Chem.*
- *Soc. Faraday Trans.* **93**, 4177–4182 (1997).
- 573 25. Barisci*, J. N., Wallace*, G. G. & Baughman, R. H. Electrochemical studies of single-wall carbon
- nanotubes in aqueous solutions. J. Electroanal. Chem. 488, 92–98 (2000).
- 575 26. Barisci, J. N., Wallace, G. G., MacFarlane, D. R. & Baughman, R. H. Investigation of ionic liquids
- as electrolytes for carbon nanotube electrodes. *Electrochem. commun.* **6**, 22–27 (2004).
- 577 27. Senokos, E. et al. Energy storage in structural composites by introducing CNT fiber/polymer
- 578 electrolyte interleaves. *Sci. Rep.* **8**, 1–10 (2018).
- 579 28. Lian, K. & Li, C. Heteropoly Acid Electrolytes for Double-Layer Capacitors and
- Pseudocapacitors. *Electrochem. Solid-State Lett.* **11**, A158 (2008).
- 581 29. Gao, H. & Lian, K. High rate all-solid electrochemical capacitors using proton conducting
- polymer electrolytes. *J. Power Sources* **196**, 8855–8857 (2011).
- 583 30. Sharma, P. & Bhatti, T. S. A review on electrochemical double-layer capacitors. *Energy Convers*.

- 584 *Manag.* **51**, 2901–2912 (2010).
- 585 31. Frackowiak, E. & Béguin, F. Carbon materials for the electrochemical storage of energy in capacitors. *Carbon N. Y.* **39**, 937–950 (2001).
- Bard, A. J. & Faulkner, L. R. Electrochemical methods: Fundamentals and applications. (JOHN
 WILEY & SONS, INC., 2001).
- Burt, R., Birkett, G. & Zhao, X. S. A review of molecular modelling of electric double layer capacitors. *Phys. Chem. Chem. Phys.* **16**, 6519 (2014).
- 591 34. Yamamoto, R. *et al.* External electric field dependence of the structure of the electric double layer at an ionic liquid/Au interface. *Appl. Phys. Lett.* **101**, 053122 (2012).
- 593 35. Vatamanu, J., Borodin, O. & Smith, G. D. Molecular insights into the potential and temperature dependences of the differential capacitance of a room-temperature ionic liquid at graphite electrodes. *J. Am. Chem. Soc.* **132**, 14825–14833 (2010).
- Vatamanu, J., Borodin, O., Olguin, M., Yushin, G. & Bedrov, D. Charge storage at the nanoscale:
 understanding the trends from the molecular scale perspective. *J. Mater. Chem. A* 5, 21049–21076
 (2017).
- Wang, Y., Qian, C., Huo, F., Qin, J. & He, H. Molecular mechanism of anion size regulating the nanostructure and charging process at ionic liquid-electrode interfaces. *J. Mater. Chem. A* **8**, 19908–19916 (2020).
- Sha, M., Wu, G., Dou, Q., Tang, Z. & Fang, H. Double-layer formation of [Bmim][PF6] Ionic liquid triggered by surface negative charge. *Langmuir* **26**, 12667–12672 (2010).
- Feng, G., Huang, J., Sumpter, B. G., Meunier, V. & Qiao, R. Structure and dynamics of electrical double layers in organic electrolytes. *Phys. Chem. Chem. Phys.* **12**, 5468–5479 (2010).

- Jo, S., Park, S.-W., Shim, Y. & Jung, Y. Effects of Alkyl Chain Length on Interfacial Structure
 and Differential Capacitance in Graphene Supercapacitors: A Molecular Dynamics Simulation
 Study. *Electrochim. Acta* 247, 634–645 (2017).
- Henderson, D. & Boda, D. Insights from theory and simulation on the electrical double layer.
 Phys. Chem. Chem. Phys. 11, 3822–3830 (2009).
- Noh, C. & Jung, Y. Understanding the charging dynamics of an ionic liquid electric double layer capacitor: Via molecular dynamics simulations. *Phys. Chem. Chem. Phys.* **21**, 6790–6800 (2019).
- Demir, B. & Searles, D. J. Investigation of the ionic liquid graphene electric double layer in
 supercapacitors using constant potential simulations. *Nanomaterials* 10, 1–27 (2020).
- Liu, X., Wang, Y., Li, S. & Yan, T. Effects of anion on the electric double layer of imidazolium-based ionic liquids on graphite electrode by molecular dynamics simulation. *Electrochim. Acta* 184, 164–170 (2015).
- Jiang, G., Cheng, C., Li, D. & Liu, J. Z. Molecular dynamics simulations of the electric double
 layer capacitance of graphene electrodes in mono-valent aqueous electrolytes. *Nano Res.* 9, 174–
 186 (2016).
- Feng, G. *et al.* The importance of ion size and electrode curvature on electrical double layers in ionic liquids. *Phys. Chem. Chem. Phys.* **13**, 1152–1161 (2011).
- Feng, G., Li, S., Zhao, W. & Cummings, P. T. Microstructure of room temperature ionic liquids at stepped graphite electrodes. *AIChE J.* **61**, 3022–3028 (2015).
- 48. Ma, J. Le, Meng, Q. & Fan, J. Charge driven lateral structural evolution of ions in electric double
 layer capacitors strongly correlates with differential capacitance. *Phys. Chem. Chem. Phys.* 20,
 8054–8063 (2018).
- 49. Patra, S. et al. Mechanistic insight into the improved Li ion conductivity of solid polymer

- 629 electrolytes. RSC Adv. 9, 38646–38657 (2019).
- 630 50. Jewett, A. I. et al. Moltemplate: A Tool for Coarse-Grained Modeling of Complex Biological
- Matter and Soft Condensed Matter Physics. J. Mol. Biol. 433, 166841 (2021).
- 632 51. Plimpton, S. Fast Parallel Algorithms for Short-Range Molecular Dynamics. J. Comput. Phys.
- 633 **117**, 1–19 (1995).
- 634 52. Allouche, A. Gabedit-A graphical user interface for computational chemistry softwares. J.
- 635 *Comput. Chem.* **32**, 174–182 (2011).
- 636 53. Hardy, D. J., Stone, J. E. & Schulten, K. Multilevel summation of electrostatic potentials using
- graphics processing units. *Parallel Comput.* **35**, 164–177 (2009).
- 638 54. Wang, Z., Yang, Y., Olmsted, D. L., Asta, M. & Laird, B. B. Evaluation of the constant potential
- method in simulating electric double-layer capacitors. J. Chem. Phys. 141, 184102 (2014).
- 640 55. Merlet, C. et al. Simulating Supercapacitors: Can We Model Electrodes As Constant Charge
- 641 Surfaces? J. Phys. Chem. Lett. 4, 264–268 (2013).
- 56. Frolov, A. I., Kirchner, K., Kirchner, T. & Fedorov, M. V. Molecular-scale insights into the
- mechanisms of ionic liquids interactions with carbon nanotubes. Faraday Discuss. 154, 235–247
- 644 (2012).
- 57. Shim, Y., Kim, H. J. & Jung, Y. Graphene-based supercapacitors in the parallel-plate electrode
- configuration: Ionic liquids versus organic electrolytes. *Faraday Discuss.* **154**, 249–263 (2012).
- 647 58. Glendening, E. D. & Streitwieser, A. Natural energy decomposition analysis: An energy
- partitioning procedure for molecular interactions with application to weak hydrogen bonding,
- strong ionic, and moderate donor–acceptor interactions. J. Chem. Phys. 100, 2900–2909 (1994).
- 650 59. Glendening, E. D. Natural Energy Decomposition Analysis: Explicit Evaluation of Electrostatic

- and Polarization Effects with Application to Aqueous Clusters of Alkali Metal Cations and
- Neutrals. J. Am. Chem. Soc. 118, 2473–2482 (1996).
- 653 60. Schenter, G. K. & Glendening, E. D. Natural Energy Decomposition Analysis: The Linear
- Response Electrical Self Energy. *J. Phys. Chem.* **100**, 17152–17156 (1996).
- 655 61. Barca, G. M. J. et al. Recent developments in the general atomic and molecular electronic
- 656 structure system. J. Chem. Phys. 152, 154102 (2020).
- 657 62. Glendening, E. D., Landis, C. R. & Weinhold, F. NBO 6.0: Natural bond orbital analysis
- 658 program. J. Comput. Chem. **34**, 1429–1437 (2013).
- 659 63. Zhao, G. & Zhu, H. Cation–π Interactions in Graphene-Containing Systems for Water Treatment
- and Beyond. *Advanced Materials* vol. 32 (2020).
- 661 64. Shi, G., Ding, Y. & Fang, H. Unexpectedly strong anion- π interactions on the graphene flakes. J.
- 662 *Comput. Chem.* **33**, 1328–1337 (2012).
- 663 65. Saha, B. & Bhattacharyya, P. K. Anion $\cdots \pi$ interaction in oxoanion-graphene complex using
- 664 coronene as model system: A DFT study. Comput. Theor. Chem. 1147, 62–71 (2019).
- 665 66. Garcia-Yoldi, I., Álvarez, F. & Colmenero, J. On the interactions between poly(ethylene oxide)
- and graphite oxide: A comparative study by different computational methods. J. Chem. Phys. 138,
- 667 94308 (2013).
- 668 67. Chaurasia, S. K., Singh, R. K. & Chandra, S. Ion-polymer and ion-ion interaction in PEO-based
- polymer electrolytes having complexing salt LiClO4 and/or ionic liquid, [BMIM][PF6]. J. Raman
- 670 *Spectrosc.* **42**, 2168–2172 (2011).
- 671 68. Wander, M. C. F. & Shuford, K. L. Electrolyte effects in a model system for mesoporous carbon
- 672 electrodes. J. Phys. Chem. C 115, 4904–4908 (2011).

- 673 69. Marti, J., Nagy, G., Gordillo, M. C. & Guàrdia, E. Molecular simulation of liquid water confined 674 inside graphite channels: Thermodynamics and structural properties. *J. Chem. Phys.* **124**, 94703 675 (2006).
- Cagle, C. *et al.* Structure and charging kinetics of electrical double layers at large electrode
 voltages. *Microfluid. Nanofluidics* 8, 703–708 (2010).
- 71. Cui, S. T. & Cochran, H. D. Molecular dynamics simulation of interfacial electrolyte behaviors in nanoscale cylindrical pores. *J. Chem. Phys.* **117**, 5850–5854 (2002).
- 680 72. Georgi, N., Kornyshev, A. A. & Fedorov, M. V. The anatomy of the double layer and capacitance 681 in ionic liquids with anisotropic ions: Electrostriction vs. lattice saturation. *J. Electroanal. Chem.* 682 **649**, 261–267 (2010).
- Vatamanu, J., Borodin, O. & Smith, G. D. Molecular simulations of the electric double layer structure, differential capacitance, and charging kinetics for N-methyl-N-propylpyrrolidinium bis(fluorosulfonyl)imide at graphite electrodes. *J. Phys. Chem. B* **115**, 3073–3084 (2011).
- Desai, T. G. Molecular dynamics study of screening at ionic surfaces. *J. Chem. Phys.* 127, 154707
 (2007).
- Donoso, J. P. *et al.* Nuclear magnetic relaxation study of poly(ethylene oxide)–lithium salt based electrolytes. *J. Chem. Phys.* **98**, 10026–10036 (1993).
- Siqueira, L. J. A. & Ribeiro, M. C. C. Molecular dynamics simulation of the polymer electrolyte
 poly(ethyleneoxide)/LiClO4. I. Structural properties. *J. Chem. Phys.* 122, 194911 (2005).
- Yang, H. et al. Gel polymer dominated ion charging mechanisms within graphene nanochannels.
 J. Power Sources 541, 231684 (2022).
- Nihonyanagi, S. *et al.* Potential-dependent structure of the interfacial water on the gold electrode.

 in *Surface Science* vol. 573 11–16 (2004).

- Hasan, M. H. & McCrum, I. T. Understanding the role of near-surface solvent in electrochemical
 adsorption and electrocatalysis with theory and experiment. *Curr. Opin. Electrochem.* 33, 100937
 (2022).
- 80. Park, S.-H. & Sposito, G. Structure of Water Adsorbed on a Mica Surface. *Phys. Rev. Lett.* 89,
 85501 (2002).
- 701 81. Cheng, L., Fenter, P., Nagy, K. L., Schlegel, M. L. & Sturchio, N. C. Molecular-Scale Density

 702 Oscillations in Water Adjacent to a Mica Surface. *Phys. Rev. Lett.* 87, 156103 (2001).
- Yang, H., Bo, Z., Yang, J., Yan, J. & Cen, K. Towards understanding the effects of van der Waals strengths on the electric double-layer structures and capacitive behaviors. *J. Power Sources* **366**, 218–225 (2017).
- 706 83. Zhang, S. *et al.* Insights into the effects of solvent properties in graphene based electric double-707 layer capacitors with organic electrolytes. *J. Power Sources* **334**, 162–169 (2016).
- Jiang, D. & Wu, J. Unusual effects of solvent polarity on capacitance for organic electrolytes in a nanoporous electrode. *Nanoscale* **6**, 5545–5550 (2014).
- 710 85. Chandra, A. Temperature dependent ionic conductivity and cell performance studies of hot-711 pressed nanocomposite polymer electrolytes. *Compos. Commun.* **4**, 33–36 (2017).

712

713

714

715